# High pressure floating zone growth and structural properties of ferrimagnetic quantum paraelectric $BaFe_{12}O_{19}$

H. B. Cao, Z. Y. Zhao, M. Lee, et al.

View Online    Export Citation    CrossMark

## ARTICLES YOU MAY BE INTERESTED IN

A practical guide for crystal growth of van der Waals layered materials
Journal of Applied Physics 128, 051101 (2020); https://doi.org/10.1063/5.0015971

When do bubbles cause a floating body to sink?
American Journal of Physics 69, 1064 (2001); https://doi.org/10.1119/1.1383600

Giant magnetostriction effect near onset of spin reorientation in MnBi
Applied Physics Letters 112, 192411 (2018); https://doi.org/10.1063/1.5026408

# High pressure floating zone growth and structural properties of ferrimagnetic quantum paraelectric BaFe$_{12}$O$_{19}$

H. B. Cao,[1] Z. Y. Zhao,[2,3] M. Lee,[4,5] E. S. Choi,[5] M. A. McGuire,[2]
B. C. Sales,[2] H. D. Zhou,[3] J.-Q. Yan,[2,6] and D. G. Mandrus[2,6]

[1]*Quantum Condensed Matter Division, Oak Ridge National Laboratory, Oak Ridge,
Tennessee 37831, USA*
[2]*Materials Science and Technology Division, Oak Ridge National Laboratory, Oak Ridge,
Tennessee 37831, USA*
[3]*Department of Physics and Astronomy, University of Tennessee, Knoxville,
Tennessee 37996, USA*
[4]*Department of Physics, Florida State University, Tallahassee, Florida 32306-3016, USA*
[5]*National High Magnetic Field Laboratory, Florida State University, Tallahassee,
Florida 32310-3706, USA*
[6]*Department of Materials Science and Engineering, University of Tennessee, Knoxville,
Tennessee 37996, USA*

High quality single crystals of BaFe$_{12}$O$_{19}$ were grown using the floating zone technique in 100 atm of flowing oxygen. Single crystal neutron diffraction was used to determine the nuclear and magnetic structures of BaFe$_{12}$O$_{19}$ at 4 K and 295 K. At both temperatures, there exist local electric dipoles formed by the off-mirror-plane displacements of magnetic Fe$^{3+}$ ions at the bipyramidal sites. The displacement at 4 K is about half of that at room temperature. The temperature dependence of the specific heat shows no anomaly associated with long range polar ordering in the temperature range from 1.90 to 300 K. The inverse dielectric permittivity, $1/\varepsilon$, along the $c$-axis shows a $T^2$ temperature dependence between 10 K and 20 K, with a significantly reduced temperature dependence displayed below 10 K. Moreover, as the sample is cooled below 1.4 K there is an anomalous sharp upturn in $1/\varepsilon$. These features resemble those of classic quantum paraelectrics such as SrTiO$_3$. The presence of the upturn in $1/\varepsilon$ indicates that BaFe$_{12}$O$_{19}$ is a critical quantum paraelectric system with Fe$^{3+}$ ions involved in both magnetic and electric dipole formation. *© 2015 Author(s). All article content, except where otherwise noted, is licensed under a Creative Commons Attribution 3.0 Unported License.* [http://dx.doi.org/10.1063/1.4922934]

Quantum paraelectricity has been an interesting topic for decades. A well-known case is SrTiO$_3$, which displays a very large dielectric constant at low temperatures but fails to go through a ferroelectric transition due to quantum fluctuations associated with the zero point energy.[1] The quantum paraelectric state is fragile and can be tuned to the ferroelectric state with a small stimulus such as quenched disorder, isotopic substitution, and external stress.[2–6] Quantum paraelectrics, therefore, provide unique examples to study quantum phase transitions that may underlie much universal behavior.[7]

Combining magnetism with quantum paraelectricity is a topic of lively recent interest. EuTiO$_3$, with magnetic Eu$^{2+}$ ions replacing nonmagnetic Sr$^{2+}$, has attracted considerable attention as an antiferromagnetic quantum paraelectric system, in which magnetism can be employed as a parameter to tune the dielectric response.[8] The delicate balance in EuTiO$_3$ between para- and ferroelectricity, and between anti- and ferromagnetic ordering, was demonstrated recently by the simultaneous realization of ferromagnetism and ferroelectricity in strained EuTiO$_3$ thin films.[9] Magnetic quantum paraelectrics are, therefore, important for both fundamental physics and technological applications.

Recently BaFe$_{12}$O$_{19}$, a well-known ferrite permanent magnet with $T_C$ above 720 K, was proposed to exhibit quantum paraelectric behavior.[10] BaFe$_{12}$O$_{19}$ is an important member of the

hexagonal ferrites, also known as hexaferrites, discovered in 1950s.[11–15] It has been widely used as a permanent magnet, in magnetic recording media, in microwave devices, and also for fabricating multiferroic devices.[15–19] $BaFe_{12}O_{19}$ crystallizes in the centrosymmetric magnetoplumbite structure with space group $P6_3/mmc$. As shown in Fig. 1, the magnetic $Fe^{3+}$ ions occupy five different crystallographic sites: octahedral sites ($2a$, $4f$, and $12k$), tetrahedral ($4f$) sites, and trigonal bipyramidal (TBP) $4e$ sites. In the hexaferrites, all the structures can be obtained by stacking the S, R, and T blocks. Here the S, R, and T blocks are made of two, three, or four oxygen layers, respectively. $BaFe_{12}O_{19}$ has a stacking sequence of SRS*R*S. The * symbol means that the preceding block is turned 180° around the hexagonal $c$ axis. A collinear ferrimagnetic structure forms below $T_C = 723$ K with the moment direction parallel to the hexagonal $c$ axis.[20–22] The $Fe^{3+}$ magnetic moments at two $4f$ sites are antiparallel to those at the other sites ($2a$, $4e$, and $12k$), with a high spin state, which yields a net moment of up to 40 $\mu_B$ per unit cell.

The TBP $Fe^{3+}$ ions show unusual off-mirror-plane (OMP) displacements which result in local electric dipoles.[10,19,23] Neutron powder diffraction measurements suggested that the OMP displacement of TBP $Fe^{3+}$ ion is 0.26 Å in the paramagnetic phase at 743 K, and the TBP $Fe^{3+}$ ions freeze on the mirror-plane at 4.2 K.[22] The freezing of the TBP $Fe^{3+}$ ions at low temperatures agrees with a Mössbauer study reported by Mamalui *et al.*[24] However, in a later Mössbauer study, the OMP
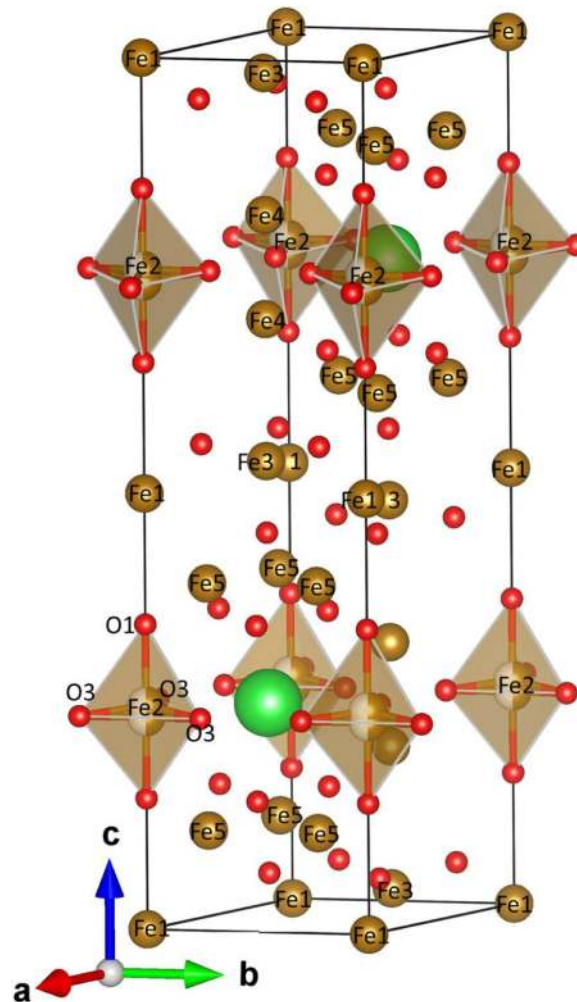


FIG. 1. The nuclear structure of $BaFe_{12}O_{19}$ showing the five Fe sites. The Fe2 atoms occupy the trigonal bipyramidal sites. $Fe^{3+}$ ions at TBP sites displace away from the mirror plane. The brown balls represent Fe and are labeled by number. The red and green balls represent O and Ba, respectively. The partially filled brown balls represent half occupied sites.

displacement was found to be nonzero and to increase linearly upon warming in the temperature range from 4 K to 300 K. The room temperature OMP displacement of 0.185 Å is consistent with an X-ray measurement[25] and another Mössbauer measurement.[26] It is still not clear whether the TBP $Fe^{3+}$ ions freeze in the mirror plane at low temperatures. Very recently, a Monte Carlo simulation predicted that antiferroelectric (AFE) order takes place below 3 K in $BaFe_{12}O_{19}$.[23] However, a later permittivity measurement did not find electric dipole order above 2 K, but did reveal a plateau feature that was attributed to the suppression of the long range electric dipole order by quantum fluctuations.[10] Therefore, it is important to resolve the discrepancy about the OMP displacements of the TBP Fe ions at low temperatures in order to understand the low temperature dielectric properties.

In this paper, we report a detailed neutron diffraction study of $BaFe_{12}O_{19}$ single crystals grown by a high pressure floating zone technique. The neutron diffraction study shows that the OMP displacements of TBP $Fe^{3+}$ ions at 4 K are nonzero, and about half of the displacement value at 300 K. The reduced OMP displacement is accompanied by a displacement of the apical oxygen ions toward the TBP Fe ions. We also studied the dielectric properties of $BaFe_{12}O_{19}$ single crystals at temperatures down to 0.4 K in order to look for any possible antiferroelectric order. The temperature dependence of the dielectric response shows an unconventional $T^2$ dependence of the inverse dielectric function from 10 to 20 K and an anomalous upturn below 1.40 K extending to the millikelvin range. Our results provide strong evidence that $BaFe_{12}O_{19}$ is simultaneously a ferrimagnet and a quantum paraelectric.

$BaFe_{12}O_{19}$ powder was synthesized by conventional solid-state reaction of appropriate mixtures of $BaCO_3$ (Alfa, 99.99%) and $Fe_2O_3$ (Alfa, 99.995%) at 1100 °C for 72 h with intermediate grindings. The $BaFe_{12}O_{19}$ feed rods used for the single crystal growth were made by pressing powder under hydrostatic pressure and then annealing these rods at 1200 °C in air. Single crystals with dimensions of 5 mm in diameter by 60 mm long were grown by the floating zone method in flowing $O_2$ atmosphere at a pressure of 100 atm. The gas flow rate was 0.2 l/min. The high pressure floating zone growth was performed using a vertical optical image furnace (Model HKZ, SciDre, GmbH, Dresden) equipped with a 5 KW xenon arc lamp. During crystal growth, the upper and lower rods were counter-rotated at a relative speed of 25 rpm in order to maintain a homogeneous melt. The crystal was grown at a rate of 6 mm/h.

Measurements of the magnetic properties were performed in a Quantum Design (QD) Magnetic Property Measurement System. The temperature dependence of the electrical resistivity and heat capacity was measured using a QD Physical Property Measurement System. A conventional four-probe technique was employed for the resistivity measurements. Pt wires were attached to rectangular bars cut from the bulk crystal using silver epoxy.

For the dielectric function measurements, a single-crystal sample was polished into a plate with typical dimensions of $4 \times 4 \times 0.1$ mm$^3$ to have a parallel-plate capacitor geometry. The plate was cut perpendicular to the *c*-axis. The electrical contacts were made by coating the two flat surfaces with silver epoxy. The capacitance of the sample was measured with an Andeen-Hagerling AH-2700A capacitance bridge, and the dielectric function was obtained by approximating the sample as an ideal parallel-plate capacitor.

Single-crystal neutron diffraction measurements were performed on the HB-3A four-circle diffractometer at the High Flux Isotope Reactor, Oak Ridge National Laboratory. A neutron wavelength of 1.003 Å was used, obtained from a bent perfect Si-331 monochromator.[27] Rietveld refinements were performed using FullProf.[28] A maximum entropy method (MEM) analysis was carried out to obtain the nuclear density map using the Dysnomia software package.[29]

Under one atmosphere of oxygen, $BaFe_{12}O_{19}$ decomposes into $BaFe_{18}O_{27}$ (the so-called *W*-phase) and other oxides before melting. This incongruent melting can be suppressed by high pressure oxygen, and congruently melting behavior was reported above 50 atm of oxygen.[30,31] Since the capability of maintaining 50 atm oxygen pressure is absent in most growth laboratories, $BaFe_{12}O_{19}$ crystals and doped variants have been mainly grown with flux techniques.

The Model HKZ high pressure image furnace enables crystal growth in controlled atmosphere at pressures up to 150 atm. The high pressure capability can be used to suppress the evaporation loss of volatile components and tune the oxygen content in oxides. The floating zone growth of

$BaFe_{12}O_{19}$ in high oxygen pressure provides a good example that high oxygen pressure can be used to modify the phase stability in $P - T - x$ space.

To obtain a high quality crystal, growth parameters such as oxygen pressure, flow rate, growth rate, and the rotation speed of both feed and seed rods, and temperature profile, are optimized. It was found that an oxygen pressure of 50 atm is necessary to obtain the right phase and maintain a stable growth. The effect of the oxygen pressure was tested and once the growth was performed in oxygen pressure below 50 atm, the as-grown ingot contains iron oxides ($Fe_2O_3$ and/or $Fe_3O_4$ depending on the oxygen pressure and temperature) and $BaFe_{18}O_{27}$ crystals with the largest dimension up to 8 mm. Room temperature X-ray diffraction performed on pulverized single crystals confirmed that $BaFe_{18}O_{27}$ is phase pure with the correct lattice parameters.

A stable growth was obtained for $BaFe_{12}O_{19}$ in an oxygen pressure of 50-100 atm with a steady flow rate of 0.2 l/min. Crystals grown with a growth rate of 4-10 mm/h are of similar quality. The rotation speed of feed and seed rods showed little effect on the growth stability. The room temperature X-ray powder diffraction pattern was collected on pulverized single crystals. No extra reflections were observed. The crystal quality was further confirmed with X-ray Laue diffraction (see supplementary material[32]).

Room temperature magnetization measurements were carried out on both $BaFe_{12}O_{19}$ and $BaFe_{18}O_{27}$ crystals. The results are shown in Fig. 2. Measurements were conducted both with the field applied along the easy axis of magnetization, the *c*-axis in these hexagonal materials, and with the field perpendicular to this axis, in the *ab*-plane. The measured saturation magnetizations for the $BaFe_{12}O_{19}$ and $BaFe_{18}O_{27}$ crystals is 0.39 MA/m (73 emu/g, 14.5 $\mu_B$/f.u.) and 0.42 MA/m (80 emu/g, 22.4 $\mu_B$/f.u.), respectively. These values are in good agreement with accepted literature values of 0.38 MA/m for $BaFe_{12}O_{19}$ and 0.41 MA/m for $BaFe_{18}O_{27}$.[33] The anisotropy field $H_A$ can be estimated by noting the field at which the magnetization saturates in the hard direction. The data in Fig. 2 give $\mu_0H_A$ = 1.75 T for $BaFe_{12}O_{19}$ and 1.66 T for $BaFe_{18}O_{27}$. These values are somewhat larger than the literature values of 1.7 and 1.5 T, respectively.[33] This may be due to demagnetization effects, which were unaccounted for here.[33]

Figure 3 shows the temperature dependence of the specific heat of a single crystal $BaFe_{12}O_{19}$ measured in the temperature range 1.90 K–320 K. The temperature dependence and magnitude agree well with the data reported on flux-grown crystals.[10] As shown in the inset of Fig. 3, there is no observable anomaly in our measurement down to 1.9 K, indicating the absence of long-range dipolar order. This result is in contrast to the most recent Monte Carlo simulation on $BaFe_{12}O_{19}$,
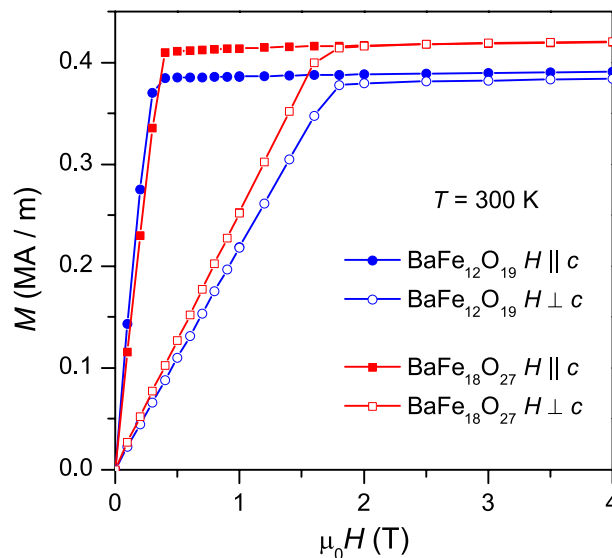


FIG. 2. Measured magnetization vs applied magnetic field for single crystals of $BaFe_{12}O_{19}$ and $BaFe_{18}O_{27}$ both parallel and perpendicular to the *c*-axis, the easy axis of magnetization.
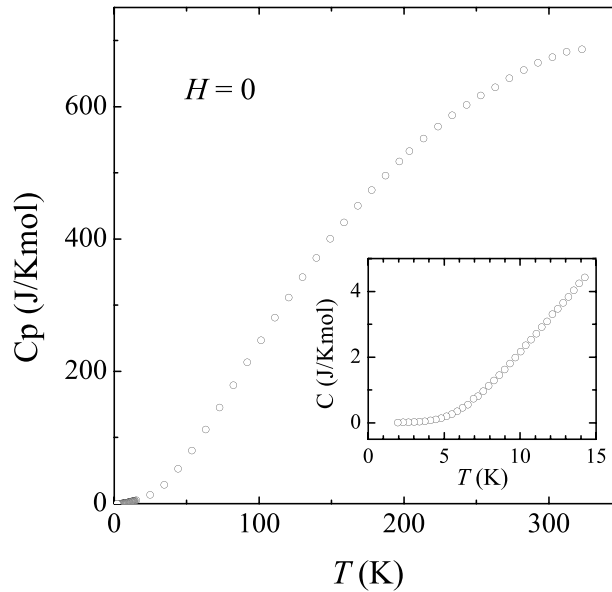
FIG. 3. Temperature dependence of specific heat in zero field. The inset shows the region below 15 K.

which predicted antiferroelectric order at 3 K.[23] Measurement in an applied magnetic field of 8 T along $c$ shows no field effect, which indicates that neither electric dipole order nor the magnetic order can be tuned by an applied magnetic field of 8 T or less along $c$.

The temperature dependence of electrical resistivity was measured in the $ab$ plane and along the $c$ axis below room temperature. The results (see supplementary material[32] for more details) show that $BaFe_{12}O_{19}$ is insulating with large anisotropy. The in-plane electrical resistivity $\rho_{ab}$ is one order of magnitude smaller than the $c$-axis electrical resistivity $\rho_c$.

A high quality $BaFe_{12}O_{19}$ single crystal was selected for neutron single crystal diffraction. More than 850 reflections were each collected at 4 K and 295 K. The structural refinements were performed to determine the nuclear and magnetic structures. The refined atomic positions and magnetic moments are listed in supplementary material.[32] Selected bond distances and angles can also be found in the supplementary material.[32] Upon cooling from 295 K to 4 K, two main changes were observed in the vicinity of the TBP sites: (1) the apical O1 shifts along $c$ towards the Fe2 ion by 0.021(3) Å (see Fig. 1). The distance between the O1 above and the O1 atom below Fe2 is reduced by 0.042(6) Å; and (2) the TBP Fe2 displaces away from the mirror plane at $z = 0.25$ by 0.177(4) Å and 0.098(9) Å at 295 K and 4 K, respectively. The OMP displacement of the TBP Fe2 is reduced upon cooling from 295 K to 4 K by 0.079(7) Å, much larger than the O1 shift, 0.021(3) Å, which is consistent with the notion that the TBP electric dipoles arise from off-centering into double wells.

To further understand the OMP displacements, we performed a MEM analysis. As shown in the nuclear density map obtained by the MEM analysis (Fig. 4), only TBP Fe ions present a large displacement along the crystallographic $c$ axis, and this displacement is reduced when cooling from 295 K to 4 K. The displacements of other atoms including the oxygen ions (O1 and O3) enclosing the TBP Fe are isotropic, exhibiting conventional thermal vibrational features. Therefore, a split TBP site along the $c$ axis is necessary for both temperatures. The nuclear density at TBP sites does not show two maxima at either temperature because our neutron diffraction data were collected under the $q$ limit of 8 Å$^{-1}$. Collection of higher $q$ reflections will be necessary to resolve the expected maxima.

The observed OMP displacement at 295 K in our study, 0.177(4) Å, agrees well with the previously reported values in a range of 0.16-0.185 Å obtained by X-ray single crystal diffraction and Mössbauer measurements.[25,26,34] At 4 K, we observed a reduced OMP displacement of 0.098(9) Å, which is consistent with the latest Mössbauer study;[34] i.e., there is no freezing of the TBP $Fe^{3+}$ ions at the mirror plane as reported in Refs. [22] and [24]. At the TBP sites, there are two bond lengths for
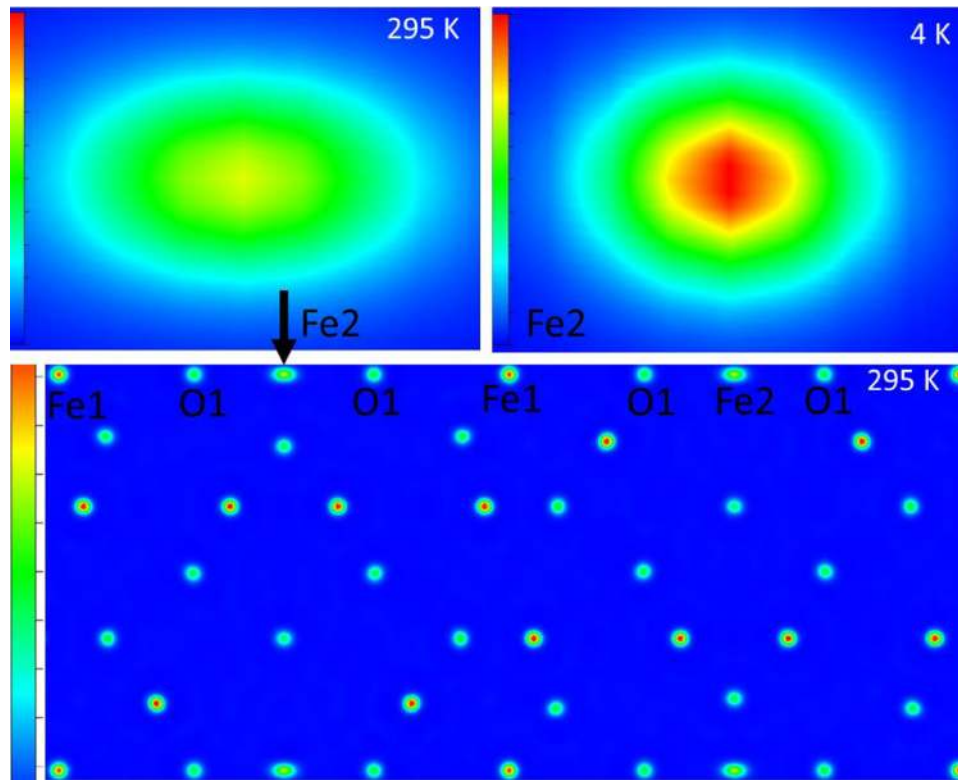
FIG. 4. Nuclear density maps of $BaFe_{12}O_{19}$: the bottom shows the full unit cell in the crystal plane (1 1 0) at the origin. The most intense sites are for $Fe^{3+}$ ions with the largest neutron scattering length. The top two panels are the nuclear density maps around the TBP Fe sites at 295 K (left) and 4 K (right).

Fe2–O1 along the $c$ axis due to the OMP displacement of Fe2: 2.486(5) Å and 2.134(5) Å at 295 K and 2.386(9) Å and 2.192(9) Å at 4 K, respectively. Both bonds are longer than the remaining Fe–O bonds at each temperature. Obviously, these two Fe2–O1 bonds show a significant temperature dependence. In contrast, the Fe2–O3 bonds in the $ab$-plane are much shorter with a length of 1.86 Å and show no temperature dependence within the error bar.

The bond lengths of in-plane Fe2–O3 bonds are close to those of the Fe–O bonds (Fe3–O4) in the tetrahedral sites. In fact, each bipyramid can be viewed as two face-sharing tetrahedra, where the TBP $Fe^{3+}$ hops from one tetrahedron to the other, forming an electric dipole. To look for possible long range order of the dipoles, high resolution data were collected with both X-ray and neutron single crystal diffraction. No peak violating the reflection condition $l = 2n$ within the space group $P6_3/mmc$ was observed with neutron single crystal diffraction at 4 K. The absence of superlattice peaks was further confirmed with X-ray single crystal diffraction measurements performed in the temperature range 28 K-300 K (results not shown). Thus, no long range antiferroelectric order forms above 4 K in $BaFe_{12}O_{19}$, consistent with the conclusion from the specific heat measurements.

Since the neutron single crystal diffraction data were collected in the magnetically ordered state at temperatures far below $T_C$, we also solved the magnetic structure with all the spins along $c$ axis (see Fig. 5). The overall magnetic structure is consistent with previous reports.[20,22] Compared to the previous neutron powder diffraction study, our single crystal study reveals a smaller magnetic moment at each $Fe^{3+}$ site at 4 K (see Table I of supplementary material[32]). The average moment size per $Fe^{3+}$ is 4.27(14) $\mu_B$, smaller than the reported 4.6(2) $\mu_B$. The net magnetic moment per $Fe^{3+}$ is 1.38(14) $\mu_B$, which is also smaller than the reported 1.7(2) $\mu_B$. Note, if all the $Fe^{3+}$ magnetic moments were constrained to have the same size in the refinements, a magnetic moment of 3.74(4) $\mu_B$ at 295 K and 4.28(4) $\mu_B$ at 4 K are obtained, which gives a net magnetic moment of 14.96(48) $\mu_B$/f.u. at 295 K (consistent with the magnetization measurement) and 17.12(17) $\mu_B$/f.u. at 4 K.
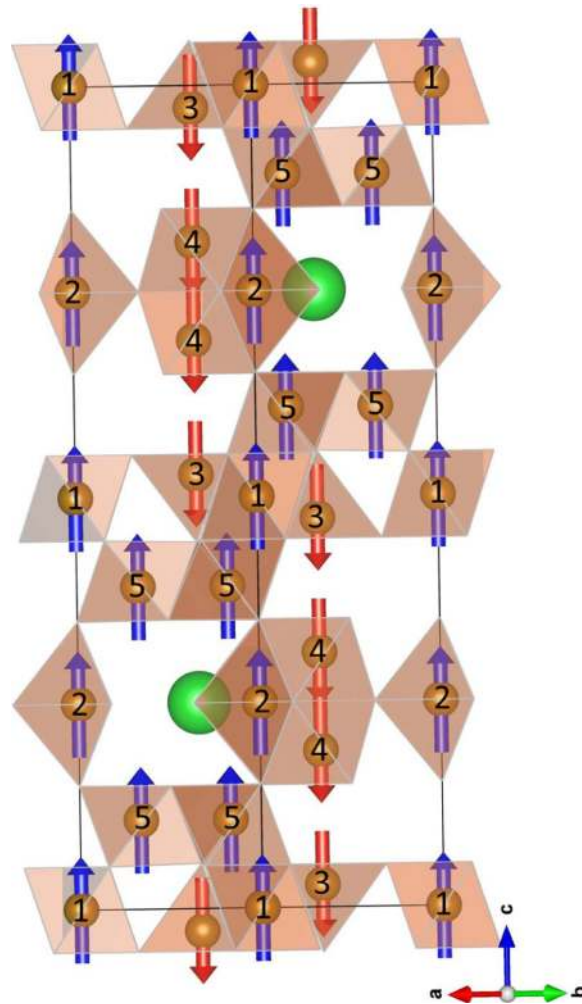
FIG. 5. The magnetic structure of $BaFe_{12}O_{19}$. Fe atoms are labeled with numbers. The moment sizes are listed in Table I of the supplementary online material.[32]

As listed in Table I of supplementary material,[32] the magnetic moments on all Fe sites increase when cooling from room temperature to 4 K. The increase is about 26% for Fe5, much larger than the 3%-10% found for the other Fe sites. This increase might be related to the displacement of O1 toward Fe2 upon cooling. As shown in Fig. 5, the TBP shares O1 with the $FeO_6$ octahedron at Fe5 sites. The displacement of O1 toward Fe2 has little effect on the positions of other five oxygen atoms in the $Fe5O_6$ octahedron but increases the bond length of Fe5-O1. The enhanced covalency of Fe2-O1 bond is expected to reduce the magnetic moment on the Fe2 site, whereas the displacement of O1 away from Fe5 favors the moment on Fe5 site. This analysis is supported by a larger moment increase of Fe5 when cooling from room temperature to 4 K as shown in Table I of supplementary material.[32] Therefore, the local structural distortion may affect both the local dipoles and the ordered magnetic moments.

A recent first principles calculation predicted AFE order at 3 K. However, no evidence was found for AFE order in the temperature dependence of the specific heat or permittivity measured on flux-grown crystals.[10] We therefore measured the dielectric function of our crystals grown by high pressure floating zone technique in the temperature range 0.4-25 K. Above 2 K, the magnitude and temperature dependence of the permittivity agree well with the previous report.[10] The permittivity increases with decreasing temperature and saturates below about 10 K. No anomaly associated with the predicted AFE order was observed. Figure 6 shows the inverse dielectric constant ($1/\varepsilon$) plotted against $T^2$. Three features are noteworthy: (1) $1/\varepsilon$ follows a $T^2$ temperature dependence in the range
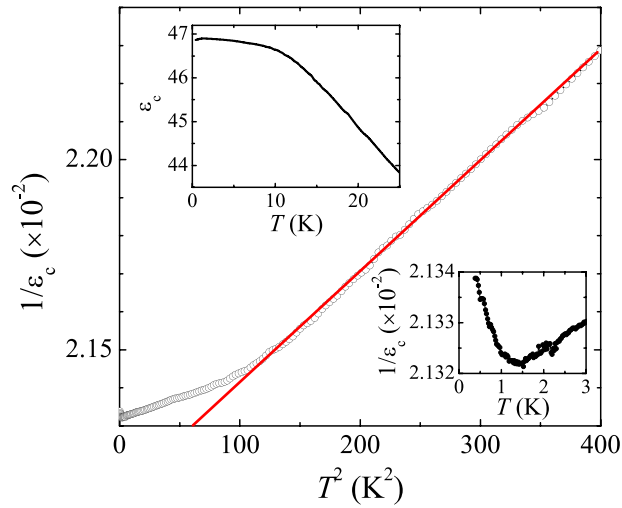
FIG. 6. $T^2$ dependence of inverse dielectric function $1/\varepsilon$ from 10 to 20 K. The upper inset shows the temperature dependence of $\varepsilon$. The lower inset highlights the anomalous upturn of $1/\varepsilon$ below 1.4 K.

10-20 K; (2) below 10 K, $1/\varepsilon$ deviates from this $T^2$ behavior, while $\varepsilon$ shows a plateau (see the top inset of Fig. 6); (3) below 1.4 K, $1/\varepsilon$ shows an anomalous upturn (see lower inset of Fig. 6) which extends down to 0.4 K, the lowest temperature measured.

A regular Curie-Weiss law cannot describe the temperature dependence of the dielectric function, especially the plateau-like feature at low temperatures. In Ref. 10, the mean-field Barrett formula was found to describe the temperature dependence of the $c$-axis dielectric permittivity well over the whole temperature range.[44] Since the Barrett formula is often used to describe the dielectric properties of quantum paraelectrics, $BaFe_{12}O_{19}$ was, thus, proposed to be a magnetic quantum paraelectric compound.[10] Our dielectric constant data show similar temperature dependence as highlighted in the upper inset of Fig. 6, which indicates that the $BaFe_{12}O_{19}$ single crystals grown using high pressure floating zone technique used in this study show similar dielectric properties to flux-grown crystals.

The observed unconventional $T^2$ temperature dependence of the inverse dielectric function from 10 to 20 K, followed by the anomalous upturn below 1.4 K, are of particular interest. A similar behavior has been observed in $SrTiO_3$ and $KTaO_3$ quantum paraelectrics on the border of ferroelectricity.[7] Both features can be understood in terms of the theory of quantum phase transitions when extended to include the effects of long-range dipolar interactions and the coupling of the electric polarization field with acoustic phonons. A similar temperature dependence of the dielectric properties of $BaFe_{12}O_{19}$ strongly suggests that $BaFe_{12}O_{19}$ is a critical quantum paraelectric system on the border of ferroelectricity.

The successful growth of $BaFe_{12}O_{19}$ single crystals demonstrates that floating zone growth under high pressure oxygen can extend the region of $P - T - x$ in which large, high quality crystals of certain materials can be grown. The floating zone method is a crucible-free growth technique which avoids crystal contamination by reaction between the melt and crucible materials. Also, floating-zone crystals are free of flux inclusions since normally no flux is used. The floating zone growth of incongruently melting materials is rather challenging. It is normally performed with a so-called traveling solvent floating zone (TSFZ) technique, in which the melt has a different composition than the desired compound. With the help of the solvent, crystals can be grown at temperatures below the decomposition temperature. Crystal growth takes place while the solvent dissolves the feed materials and precipitates on top of the seed rods. The dissolving and precipitating processes from the solvent are usually slow, thus, crystal growth with TSFZ technique is generally performed with a very slow growth rate, typically less than 1 mm/h. On the other hand, the solvent used normally has a composition different from the feed rod, thus, the as-grown crystals can be contaminated by the solvent as flux inclusions. For the growth of $BaFe_{12}O_{19}$, the applied high
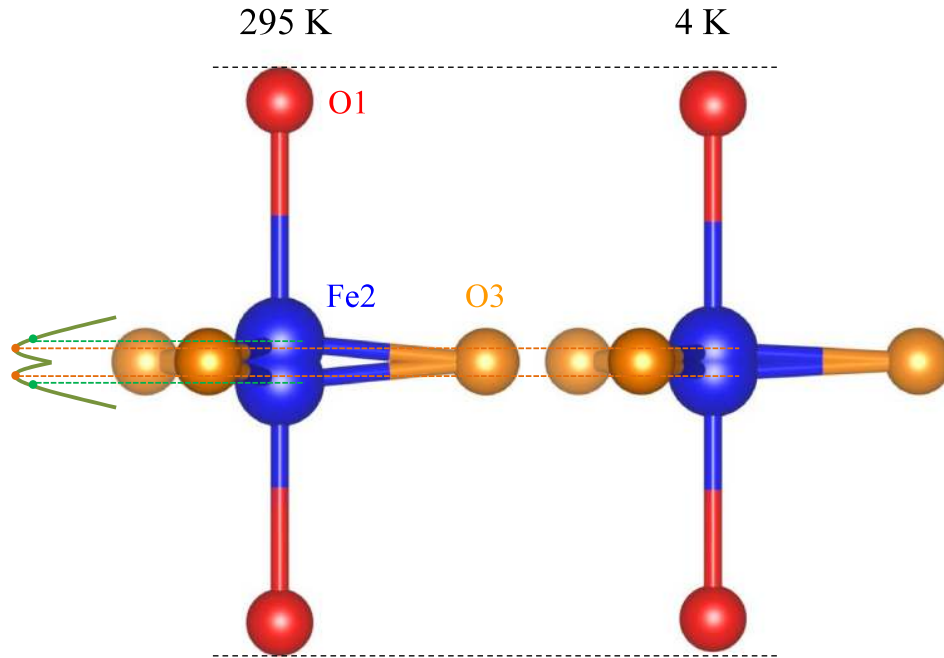
FIG. 7. Comparison of local FeO$_5$ bipyramid structure at 295 K and 4 K. The black dashed lines represent the O1 position at 295 K. Green and orange dashed lines represent the center position of the Fe2 atom at 295 K and 4 K, respectively.

oxygen pressure prevents decomposition at high temperatures. This makes possible a quick floating zone growth of large single crystals without using solvent or crucibles. Together with the recent report of successful growth of ordered anion-deficient Ca$_2$Co$_2$O$_5$ in flowing oxygen atmosphere of 145 atm,[35] our growth of BaFe$_{12}$O$_{19}$ in 100 atm oxygen suggests that the high pressure floating zone technique will be a useful tool for new and metastable materials in single crystal form.

Our neutron single crystal diffraction study confirms the OMP displacement, although reduced in magnitude, of TBP Fe ions at 4 K. We also observed the displacement of the apical O1 toward the TBP Fe. As neutrons are better than X-rays at scattering from light atoms like oxygen, it helped resolve this feature. The details of the observed local structure change around the TBP Fe site are illustrated in Fig. 7. The in-plane Fe2–O3 bonds show no temperature dependence. As highlighted by the horizontal dashed lines, the O1-O1 distance is reduced when cooling from 295 K to 4 K, resulting from the displacement of the apical O1 atoms toward Fe2. Intuitively, the displacement of O1 reduces the size of TBP which can lead to the reduced OMP displacement of Fe2. However, the OMP displacement of Fe2 is reduced by half when cooling from 295 K to 4 K, which cannot be attributed to the relatively small oxygen shift only. Instead, the oxygen shift is likely an effect of the reduced OMP displacement of Fe2.

The bipyramid can be viewed as two face-sharing tetrahedra. Each tetrahedron has a low potential center that tracks the Fe$^{3+}$ ion. Therefore, a double potential well exists (see Fig. 7) in each bipyramid site. The hopping of the TBP Fe ion between the tetrahedral site wells leads to the OMP displacement. The OMP displacement induces local electric dipoles, and the long range dipole-dipole Coulomb interaction usually stabilizes the local dipole into a ferroelectric or anti-ferroelectric order. In BaFe$_{12}$O$_{19}$, quantum fluctuations suppress the long range dipole order and no electric order has been observed down to temperatures of 0.4 K. At high temperature, a larger OMP Fe$^{3+}$ displacement was observed in our study and a Mössbauer study,[34] which indicates an anharmonic oscillator potential as shown in Fig. 7. Different from the constant equilibrium position found in a harmonic oscillator potential, the equilibrium position shifts away from the center at higher energy, i.e., higher temperature, as found here. Strong anharmonic vibrations of iron ions were also indicated in polarized infrared spectroscopy measurements.[36]

One question that remains is whether the displacement change of O1 and Fe2 upon cooling is continuous or discontinuous. The absence of any noticeable anomaly in the temperature dependence
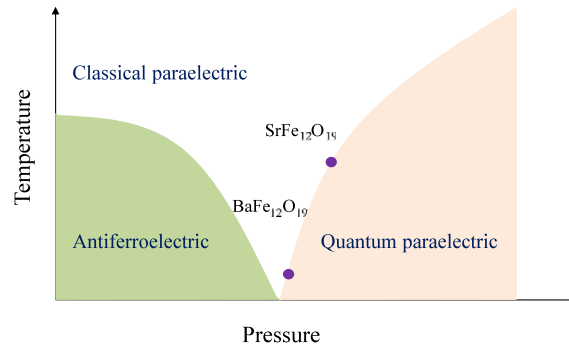
FIG. 8. Schematic temperature-pressure phase diagram in $M$-type hexaferrites. The purple points were obtained by tracking the endpoint of the $T^2$ dependence.

of specific heat and electrical resistivity suggests that the displacement takes place in a continuous manner. This is consistent with the Mössbauer study showing a continuous decrease of TBP Fe2 displacement upon cooling.[34] To further confirm this, we monitored the evolution with temperature of the integrated intensity of (0 0 22) reflection in the temperature range 4 K-300 K with single crystal neutron diffraction. The (0 0 22) peak shows a larger intensity change than other reflections we investigated. The intensity increases also in a continuous manner upon cooling from room temperature (results not shown).

The temperature dependence of the dielectric function, especially the unconventional $T^2$ temperature dependence of the inverse dielectric function below 20 K and an anomalous upturn below 1.40 K, strongly suggests that $BaFe_{12}O_{19}$ is a ferrimagnetic quantum paraelectric system on the verge of ferroelectricity. It is, in general, rare to find an ion that can play both magnetic and ferroelectric roles due to the empirical "d0-ness" rule in transition metal oxides.[37,38] The problem comes from the fact that the formation of electric dipoles usually requires hybridization between empty $d$-orbitals of cations and the filled $2p$ oxygen orbitals, while the magnetic properties derive from partially filled $d$-orbitals. Recently, perovskite manganites, $AMnO_3$ (A = Ca, Sr, Ba), were studied both theoretically and experimentally and the shift of magnetic $Mn^{4+}$ ions in $MnO_6$ octahedra was found to produce electric dipoles.[39–43] In $BaFe_{12}O_{19}$, the TBP Fe ions contribute to both magnetic and local dipoles. It thus provides another materials platform which can be tuned to optimize the cross-coupling between magnetism and ferroelectricity.

A recent study of dielectric properties of $Ba_{1-x}Sr_xFe_{12}O_{19}$ suggests that the local dipole moment decreases dramatically with the substitution of Ba by Sr.[10] The reduced dipole moment is accompanied by the suppressed displacement of TBP Fe ions. This signals the importance of the displacement of TBP Fe ions for the dielectric properties of hexaferrites. It also indicates that $SrFe_{12}O_{19}$ is further away from the antiferroelectric border, as schematically demonstrated in Fig. 8. With stress engineering, as suggested in Ref. 19, it might be possible to realize room temperature multiferroics by tuning the OMP displacement.

In summary, high quality single crystals of $BaFe_{12}O_{19}$ were grown using the floating zone technique in 100 atm of flowing oxygen. Single crystal neutron diffraction confirmed that the displacement of TBP Fe ions decreases continuously with decreasing temperature. The displacement at 4 K is nonzero and about half of that at room temperature. The reduced displacement of TBP Fe ions is accompanied by the oxygen displacement toward the TBP Fe ions. The temperature dependence of the dielectric function shows a unconventional $T^2$ temperature dependence of the inverse dielectric function below 20 K and an anomalous upturn below 1.40 K extending to the millikelvin range. These results provide strong evidence that $BaFe_{12}O_{19}$ is a ferrimagnetic quantum paraelectric compound on the border of ferroelectricity. As the TBP Fe ions contribute to both magnetism and electric dipoles, $BaFe_{12}O_{19}$ offers an ideal materials platform for tuning the coupling of magnetism and ferroelectricity.

[1] K. A. Müller and H. Burkard, Phys. Rev. B **19**, 3593 (1979).

[2] A. F. Devonshire, "Theory of ferroelectrics," Adv. Phys. **3**, 85 (1954).

[3] J. G. Bednorz and K. A. Müller, Phys. Rev. Lett. **52**, 2289 (1984).

[4] C. Ang *et al.*, J. Phys. Chem. Solids **61**, 191 (2000).

[5] M. Itoh *et al.*, Phys. Rev. Lett. **82**, 3540 (1999).

[6] J. H. Haeni *et al.*, Nature **430**, 758 (2004).

[7] S. E. Rowley, L. J. Spalek, R. P. Smith, M. P. M. Dean, M. Itoh, J. F. Scott, G. G. Lonzarich, and S. S. Saxena, Nat. Phys. **10**, 367 (2014).

[8] T. Katsufuji and H. Takagi, Phys. Rev. B **64**, 054415 (2001).

[9] J. H. Lee *et al.*, Nature **466**, 954 (2010).

[10] S. P. Shen, Y. S. Chai, J. Z. Cong, P. J. Sun, J. Lu, L. Q. Yan, S. G. Wang, and Y. Sun, Phys. Rev. B **90**, 180404(R) (2014).

[11] J. J. Went, G. W. Rathenau, E. W. Gorter, and G. W. Van Oosterhout, Philos. Technol. Rev. **13**, 194 (1952).

[12] H. P. J. Wijn, Nature **170**, 707 (1952).

[13] P. B. Braun, Nature **170**, 708 (1952).

[14] G. H. Jonker, H. P. J. Wijn, and P. B. Braun, Philos. Technol. Rev. **18**, 145 (1956).

[15] J. Smit and H. P. J. Wijn, *Ferrites* (Philips' Technical Library, Eindhoven, 1959).

[16] H. Kojima and M. Sugimoto, in *Ferromagnetic Materials*, edited by E. P. Wohlfarth (North-Holland, Amsterdam, 1982), Vol. 3, p. 305 or 393.

[17] R. C. Pullar, "Hexagonal ferrites: A review of the synthesis, properties and applications of hexaferrite ceramics," Prog. Mater. Sci. **57**(7), 1191-1334 (2012).

[18] Y. Tokunaga, Y. Kaneko, D. Okuyama, S. Ishiwata, T. Arima, S. Wakimoto, K. Kakurai, Y. Taguchi, and Y. Tokura, Phys. Rev. Lett. **105**, 257201 (2010).

[19] G. Tan and X. Chen, J. Magn. Magn. Mater. **327**, 87 (2013).

[20] E. W. Gorter, Proc. IEE Suppl. **104B**, 255 (1957).

[21] X. Obradors, A. Collomb, M. Pernet, J. C. Joubert, and A. Isalgue, J. Magn. Magn. Mater. **44**, 118 (1984).

[22] A. Collomb, P. Wolfers, and X. Obradors, J. Magn. Magn. Mater. **62**, 57 (1986).

[23] P. S. Wang and H. J. Xiang, Phys. Rev. X **4**, 011035 (2014).

[24] Y. A. Mamalui, U. P. Romanov, and K. M. Matsievskii, Sov. Phys. Solid State **21**, 117 (1979).

[25] W. D. Townes, J. H. Fang, and A. J. Perrotta, Z. Kristallogr., Kristallgeom., Kristallphys., Kristallchem. **125**, 437 (1967).

[26] J. G. Rensen and J. S. Van Wieringen, Solid State Commun. **7**, 1139 (1969).

[27] B. C. Chakoumakos, H. B. Cao, F. Ye, A. D. Stoica, M. Popovici, M. Sundaram, W. Zhou, J. S. Hicks, G. W. Lynn, and R. A. Riedel, J. Appl. Crystallogr. **44**, 655 (2011).

[28] J. Rodriguez-Carvajal, Physica B **192**, 55 (1993).

[29] K. Momma, T. Ikeda, A. A. Belik, and F. Izumi, Powder Diffr. **28**, 184 (2013).

[30] W. P. Menashi, T. R. Aucoin, J. R. Shappirio, and D. W. Eckart, J. Cryst. Growth **20**, 68 (1973).

[31] Y. Goto and T. Takada, J. Am. Ceram. Soc. **43**, 150 (1960).

[32] See supplementary material at http://dx.doi.org/10.1063/1.4922934 for Laue diffraction pattern, electrical resistivity, and structure refinement results.

[33] R. Skomski and J. M. D. Coey, *Permanent Magnetism* (Taylor & Francis, New York, 1999).

[34] G. Albanese, A. Deriu, and D. Cabrini, Hyperfine Interact. **70**, 1087 (1992).

[35] J. Zhang, H. Zheng, C. D. Malliakas, J. M. Allred, Y. Ren, Q. A. Li, T. H. Han, and J. F. Mitchell, Chem. Mater. **26**, 7172 (2014).

[36] A. S. Mikheykin, E. S. Zhukova, V. I. Torgashev, A. G. Razumnaya, Y. I. Yuzyuk, B. P. Gorshunov, A. S. Prokhorov, A. E. Sashin, A. A. Bush, and M. Dressel, Eur. Phys. J. B **87**, 232 (2014).

[37] B. T. Matthias, Phys. Rev. **75**, 1771 (1949).

[38] N. A. Hill, J. Phys. Chem. B **104**, 6694 (2000).

[39] S. Bhattacharjee, E. Bousquet, and P. Ghosez, Phys. Rev. Lett. **102**, 117602 (2009).

[40] J. M. Rondinelli, A. S. Eidelson, and N. A. Spaldin, Phys. Rev. B **79**, 205119 (2009).

[41] J. H. Lee and K. M. Rabe, Phys. Rev. Lett. **104**, 207204 (2010).

[42] H. Sakai, J. Fujioka, T. Fukuda, D. Okuyama, D. Hashizume, F. Kagawa, H. Nakao, Y. Murakami, T. Arima, A. Q. R. Baron, Y. Naguchi, and Y. Tokura, Phys. Rev. Lett. **107**, 137601 (2011).

[43] J. Hong, A. Stroppa, J. Íñigueziguez, S. Picozzi, and D. Vanderbilt, Phys. Rev. B **85**, 054417 (2012).

[44] J. H. Barrett, Phys. Rev. **86**, 118 (1952).